RABBITT phase transition across the ionization threshold

Anatoli S. Kheifets and Alexander W. Bray
Research School of Physics and Engineering, The Australian National University, Canberra ACT 2600, Australia
(Dated: October 8, 2020)

Rich physics emerges as the result of interplay between discrete and continuous quantum states. Fano resonances, absorption spectra crossing continuously ionization thresholds, scattering phase variation determined by the number of bound states are just a few examples. A process of reconstruction of attosecond beating by interference of two-photon transitions (RABBITT) reveals a similar phenomenon. In RABBITT, primary XUV driven ionization is aided by secondary IR photon absorption or emission. The latter processes involve transitions between continuous states. We demonstrate that when RABBITT crosses the ionization threshold and proceeds via a discrete bound state, its phase makes a sudden jump which can be related to the phase of the continuous transitions above the threshold. Up to now, this phase remained undetermined experimentally and could only be estimated from simplistic theoretical models. The under-threshold RABBITT allows to measure it directly and thus to provide the most complete characterization of ionization dynamics on the attosecond time scale.

PACS numbers: 32.80.Rm, 32.80.Fb, 42.50.Hz

The interplay of discrete quantum states with their continuous counterparts results in a rich plethora of physical phenomena. Discrete states fall into continuum to form Beutler-Fano resonances which are ubiquitous in ionization [1], scattering [2], and wave propagation [3, 4]. Discrete and continuous parts of absorption spectra merge continuously across the ionization threshold [5]. Finally, the number of discrete states bound by a potential determines the scattering phases all the way from threshold to infinite energy [6, 7]. Attosecond electron dynamics driven by intense and ultra-short laser pulses presents another example when crossing threshold between the discrete and continuous parts of the spectrum results in a new physical phenomenon. In the present work we consider the process of reconstruction of attosecond beating by interference of two-photon transitions (RABBITT). In RABBITT, primary XUV driven ionization is aided by secondary IR photon absorption or emission. The latter processes involve transitions between continuous states which impart their phases into the net phase of the attosecond beating. We demonstrate that when RABBITT crosses the ionization threshold, its phase makes a sudden jump which can be related to the phase of the continuous transitions above the threshold. Up to now, this phase remained undetermined experimentally and could only be estimated from simplistic theoretical models. The under-threshold RABBITT allows to measure it directly and thus to provide the most complete characterization of ionization dynamics on the attosecond time scale.

Since their conception, two-photon interferometric techniques such as attosecond streaking (AS) [8] and RABBITT [9–11] have become indispensable tools of attosecond chronoscopy of atoms [12], molecules [13, 14] and condensed matter [15]. Both techniques exploit interference of various two-photon XUV/IR ionization processes and thus get access to their phases. Those phases are then converted to the timing information which allows to resolve photoioemission on the attosecond time scale.

In a typical RABBITT measurement, an ionizing XUV attosecond pulse train (APT) is superimposed on an attenuated and variably delayed replica of the driving IR pulse. The photoelectron spectrum produced in such an ionization process contains odd order harmonic (H) peaks and even order side bands (SB). The SB's oscillate with twice the driving laser frequency ω when the IR pulse delay τ relative to XUV APT varies:

$$\begin{aligned} S_{2q}(\tau) &= \alpha + \beta \cos(2\omega\tau + \Phi_R) \\ \Phi_{\rm R} &= \Delta\phi_{2q\pm1} + \Delta\phi_{\rm W} + \Delta\phi_{\rm cc} \ . \end{aligned} \tag{1}$$

Here α and β are constants which depend on the specific experimental conditions. The RABBITT phase $\Phi_{\rm R}$ is the sum of the phase difference between the neighboring odd harmonics ($\Delta\phi_{2q\pm1} = \phi_{2q+1} - \phi_{2q-1}$), the analogous difference of the Wigner phases ($\Delta\phi_{\rm W}$) and the difference of the continuum-continuum (CC) phases ($\Delta\phi_{\rm cc}$). The latter phase differences are converted to the corresponding time delays by a finite difference formula

$$\tau_{\rm W} = \Delta\phi_{\rm W}/(2\omega) \ , \ \tau_{\rm cc} = \Delta\phi_{\rm cc}/(2\omega) \ . \tag{2}$$

The two time delays in Eq. (2), summarily known as the atomic time delay $\tau_a = \tau_{\rm W} + \tau_{\rm cc}$, describe the group delay of the photoelectron wave packet propagating in the combined field of the ion remainder and the dressing IR field relative to the free space propagation.

The contribution of the harmonic phase to a RABBITT measurement (atto-chirp) can be eliminated by a relative measurement on two atomic levels [11, 16, 17] or two spin-split components of the same level [18] photoionized by identical harmonics. Similarly, a RABBITT measurement may involve two atomic species [19–21] or alternate directions of photoelectron emission [22–24]. However, there is no direct experimental access to the continuum-continuum phase $\phi_{\rm cc}$ which is evaluated theoretically from a simplified hydrogenic model [25]. Only in this way can the Wigner phase and the corresponding Wigner delay be accessed. Very recently, a combined $\omega/2\omega$ RABBITT measurement was proposed to extract $\tau_{\rm cc}$ [26] and some limited information on $\delta\tau_{cc}$ between various photoionization channels has been extracted experimentally [27].

In the present work, we consider the under-threshold or uRABBITT process which contains a different split of the RABBITT phase and thus allows to access $\tau_{\rm CC}$

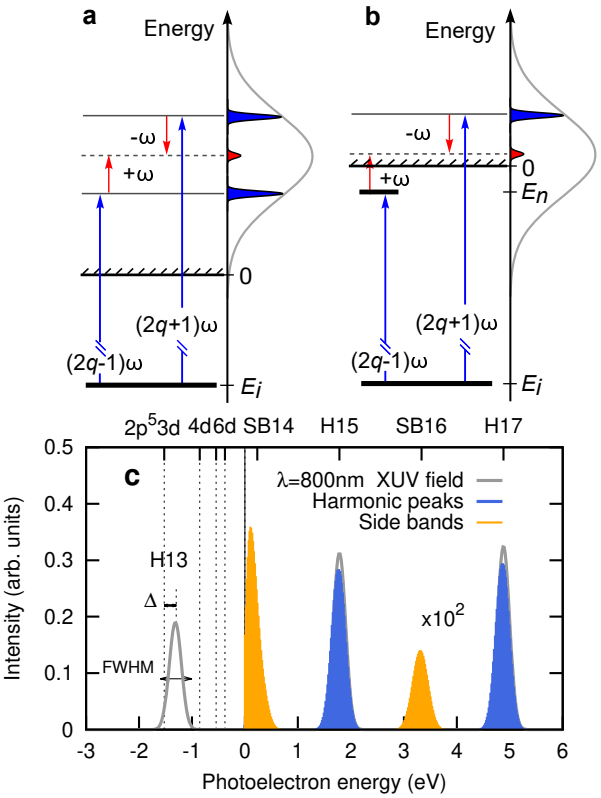

FIG. 1: (Color online) a) Schematic representation of the conventional RABBITT process (adapted from [25]). b) Same for the uRABBITT process. c) Simulated photoelectron spectrum of Ne at 800 nm overlapped with the corresponding XUV spectrum of the driving APT. Harmonics H15 and H17 are perfectly matched with the corresponding peaks of the photoelectron spectrum while H13 is found below threshold where it overlaps with the $2p^5 3d$ energy level. The spectral width (FWHM) of H13 and its detuning Δ relative to E_{3d} are shown with arrows. The SB16 (RABBITT) and SB14 (uRABBIT) are scaled up for better visibility.

experimentally. The uRABBITT process is illustrated graphically in Fig. 1b in comparison with its conventional counterpart shown in Fig. 1a. In the conventional RABBITT, the XUV photon $\Omega = (2q \pm 1)\omega$ absorbed from the initial bound state E_i is augmented by an IR photon $\mp\omega$ leading to formation of the SB of the order $2q$. In the uRABBITT process, the $(2q-1)\omega$ photon absorption promotes the target electron to a discrete excited state below the threshold $E_n < 0$. It is the subsequent ω photon absorption that takes the photoelectron to the continuum where it interferes with its downward shifted counterpart which does undergo a CC transition. While the conventional RABBITT phase contains the CC component twice, the uRABBIT phase contains only one CC component. In this respect, it is similar to AS in which the direct XUV ionization does not contain the CC phase whereas the IR aided process contains it only once.

The uRABBITT process has been demonstrated in He [28] and more recently in Ne [29], both atoms driven at 800 nm with a slight detuning in the case of He. The Ne case is illustrated in Fig. 1c where the harmonic H13 falls below the ionization threshold at $I_p = 21.56$ eV whereas SB14 emerges just above it. Absorption of an XUV photon from the harmonic H13 leads to the population of the excited $2p^5 3d$ and $2p^5 4s$ states with comparable oscillator strengths [30]. However, the IR absorption from $3d$ is much stronger than that from $4s$ and the latter state can be ignored in the uRABBITT process. The next SB16 is formed by the conventional RABBITT as both the adjacent H15 and H17 are placed well in the continuum. Thus by comparing the phase of the SB14 and SB16 oscillations as functions of the XUV/IR delay and the photoelectron emission direction we can elucidate the key distinctions between the conventional and uRABBITT processes.

Our RABBITT simulations are based on a numerical solution of the time-dependent Schrödinger equation (TDSE) in the single-active electron (SAE) approximation [31]. This approximation is valid in the photon energy range considered here which is well below the $3s$ threshold. The TDSE is driven by a superposition of the XUV APT and the IR pulses in several fixed increments of IR/XUV delay τ. The photoelectron spectrum is obtained by projecting the time-dependent wave function at the end of the evolution on the basis of Volkov states. Numerical details are given in the preceding works [32, 33]. All the numerical parameters are the same except the number of pulselets in the ATP. It is increased from 11 to 21 thus decreasing the FWHM from 0.4 to 0.2 eV.

The photoelectron peaks corresponding to SB14 and 16 (shaded in orange in Fig. 1c) are fitted with Gaussian profiles and their magnitude is analyzed using Eq. (1) as the function of the delay τ. Results of this analysis are displayed in Fig. 2 for He (left) and Ne (right). The top row of panels in Fig. 2 displays the RABBITT phases of SB16 and SB18 in He (a) and SB14 and SB16 in Ne (b). These phases are plotted versus the common axis of the photoelectron energy $E_{2q} = 2q\omega - I_p$ adjusted for each SB_{2q}. The data points are obtained by varying the central frequency of the IR pulse from 1.53 to 1.70 eV. The bottom row of Fig. 2 visualizes the position of the preceding harmonic peak $E_{2q-1} = (2q-1)\omega - I_p$ which becomes negative at the onset of the uRABBITT regime. In the bottom panels, the energy levels are marked indicating positions of the $1snp$ states in He (c) and $2p^5 nd$ states in Ar (d). At $\omega \simeq 1.55$ eV, the H15 harmonic overlaps with the $1s3p$ level in He and the H17 harmonic crosess the $2p^5 3d$ level in Ne. Close to this IR photon energy, the RABBITT phase makes a sudden jump by approximately $-\pi/2$. When an increment of 2π is added to the raw data points above 1.55 eV, they merge smoothly with the remaining data making a nearly continuous phase transition from the RABBITT to uRABBITT regime as the photon energy and the corresponding photoelectron energy decrease.

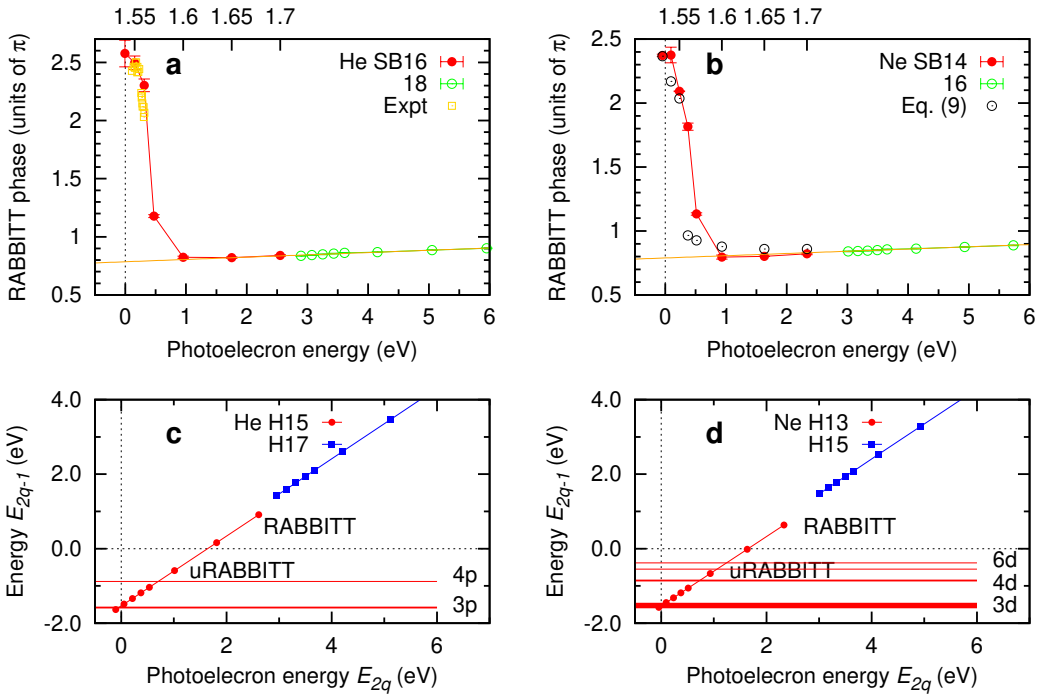

FIG. 2: Top row: the RABBITT phases of SB16 and SB18 in He (a) and SB14 and SB16 in Ne (b) are plotted as functions of the corresponding photoelectron energy $E_{2q} = 2q\omega - I_p$. The data points are obtained by sweeping the central IR frequency ω across the range $1.53 - 1.70$ eV. The solid line extrapolates the RABBITT phase towards the threshold. Experimental data for He from [28] are exhibited with orange open circles. The black open circles for Ne display predictions of Eq. (9). Bottom row: The photoelectron energy corresponding to the preceding harmonic peak $E_{2q-1} = (2q-1)\omega - I_p$. Onset of uRABBITT corresponds to $E_{2q-1} < 0$. The horizontal lines mark the energies of the bound states: $1snp$ in He (c) and $2p^5nd$ in Ne (d). The width of the line visualizes the corresponding oscillator strength for the discrete transitions from the ground state. Higher Rydberg states converging towards the threshold have much smaller oscillator strengths and are not shown.

Yet another clear distinction between the RABBITT and uRABBITT regimes is displayed in Fig. 3. Here the RABBITT phases of SB14 and 16 are plotted versus the photoelectron emission angle. The polarization direction serves as the common reference and the angular variation of the phase relative to this direction is plotted. The SB14 shows a clear evolution of its angular dependence. At $\omega = 1.55$ eV (uRABBITT regime), this phase drops down sharply by nearly one unit of π at the emission angles exceeding $\theta \simeq 40°$. At higher photon energies $\omega = 1.6$ and 1.65 eV this angular dependence becomes smooth and approaches gradually that of SB16 whose angular variation shows little change with the photon frequency in this range.

The cross-over between RABBITT and uRABBITT regimes exhibited in Figs. (2) and (3) can be understood qualitatively using the lowest order perturbation theory (LOPT) with respect to the photon-atom interaction [25, 34]. In the LOPT, the amplitude of the two-photon ionization process is written as

$$M(\boldsymbol{k}, i+\Omega) \propto \frac{1}{i}\left\{\sum_{E_\nu<0} + \int_0^\infty d\kappa^2\right\}(-i)^L e^{i\eta_L} Y_{LM}(\hat{\boldsymbol{k}}) \times \left[\frac{\langle kL\|r\|E_n\lambda\rangle\langle E_n\lambda\|r\|i\rangle}{E_i+\Omega-E_n-i\gamma} + \frac{\langle kL\|r\|\kappa\lambda\rangle\langle\kappa\lambda\|r\|i\rangle}{E_i+\Omega-\kappa^2/2-i\gamma}\right] \quad (3)$$

Here $\langle kL|$ and $\langle\kappa\lambda|$ are final and intermediate states defined by their linear and angular momenta. The reduced dipole matrix elements $\langle\|r\|\rangle$ in the above expression are made real by stripping them of the exponential phases and angular dependence. For the conventional RABBITT, the sum over discrete intermediate states is neglected in Eq. (3) as the corresponding energy denominators are large. Accordingly, the phase of the two-photon

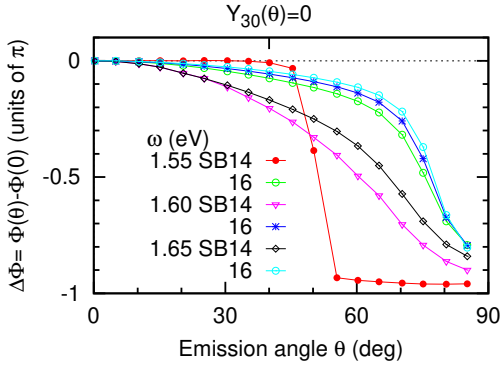

FIG. 3: (Color online) Angular variation of the RABBITT phase for SB14 and 16 relative to the polarization direction $\theta = 0$ at various photon energies. The angular position of the kinematic node in the f partial wave is marked.

amplitude becomes

$$\begin{aligned}\arg M_{2q\pm1}(k,\kappa) &= \phi_{2q\mp1} + \eta_\lambda(\kappa) + \phi_{\rm cc}(k,\kappa) \\ &+\pi - \pi\lambda/2 + \left\{\arg\left[Y_{l_i m_i}(\hat{k})\right] = 0 \;\; , \hat{k} \parallel \hat{z}\right\}\end{aligned} \tag{4}$$

Here $\phi_{2q\mp1}$ is the harmonics phase for emission (+) or absorption (−) of an IR photon, $\eta_\lambda(\kappa)$ is the XUV photoionization (Wigner) phase and $\phi_{\rm cc}(k,\kappa)$ is the CC phase. The last term in the RHS of (4) vanishes in the polarization direction. For uRABBITT, conversely, the integral can be neglected and the phase of amplitude (4) becomes

$$\begin{aligned}\arg M_{2q-1}(n,k) &= \phi_{2q-1} + \eta_L(k) - \pi(L+1)/2 + \phi_n \\ \phi_n &= \arg(E_{2q-1} - E_n - i\Gamma)^{-1} = \arctan(\Gamma/\Delta)\end{aligned} \tag{5}$$

Here we isolated a single term in the sum over the discrete intermediate states which resonates with the uRABBITT harmonic H_{2q-1} because of a small detuning $\Delta = E_{2q-1} - E_n$. We also substituted the infinitesimal γ with a finite Γ. The latter is proportional to the spectral width of the XUV field [40].

The corresponding RABBITT and uRABBITT phases are calculated as $\arg\left[M^*_{2q-1}M_{2q+1}\right]$. In RABBITT,

$$\begin{aligned}\Phi_{\rm R} &= \Delta\phi_{2q\pm1} + \eta_\lambda(\kappa_>) - \eta_\lambda(\kappa_<) \\ &+\phi_{\rm cc}(k,\kappa_>) - \phi_{\rm cc}(k,\kappa_<) \equiv \Delta\phi_{2q\pm1} + 2\omega[\tau_W(k) + \tau_{cc}(k)]\end{aligned} \tag{6}$$

Here the linear momenta in the final k and intermediate $\kappa_<, \kappa_>$ states are related by the energy conservation $\kappa_>^2/2 - k^2/2 = k^2/2 - \kappa_<^2/2 = \omega$. The corresponding phase differences are converted to the time delays using the finite difference formula (2). Analogously,

$$\begin{aligned}\Phi_{\rm uR} &= \Delta\phi_{2q'\pm1} + \eta_\lambda(p_>) - \eta_L(p) + \phi_{\rm cc}(p,p_>) + \phi_{L,\lambda} \\ &\approx \Delta\phi_{2q'\pm1} + \omega[\tau_{\rm W}(p) + \tau_{\rm cc}(p)] + \phi_{L\lambda} + \phi_n\end{aligned} \tag{7}$$

Here $\phi_{L\lambda} = \pi(L-\lambda+1)/2$ is the kinematic phase factor. Transition to the second line in Eq. (7) exploits the near-threshold scattering phase property $\eta_L(p) \approx \sigma_L(p) \approx \sigma_\lambda(p)$. The latter bare Coulomb phase is divergent near threshold independently of L [35]

$$\sigma_L(k) \simeq \eta\left[\ln\sqrt{(L+1)^2+\eta^2} - 1\right] \to \eta\ln|\eta| \;\; \forall L \; . \tag{8}$$

Here $|\eta| = 1/k \to \infty$ near the threshold. We also used an alternative definition of the CC phase in AS [25] $\tau_{\rm cc}(p) \approx \phi_{\rm cc}(p,p_>)/\omega$. This leads to the following expression for the uRABBITT/RABBITT phase difference:

$$\begin{aligned}\Phi_{\rm uR} - \Phi_{\rm R} &= \Delta\phi_{2q'\pm1} - \Delta\phi_{2q\pm1} + \omega[\tau_{\rm W}(p) + \tau_{\rm cc}(p)] \\ &\quad -2\omega[\tau_{\rm W}(k) + \tau_{\rm cc}(k)] + \phi_{L\lambda} + \phi_n \\ &\approx -\omega[\tau_W(p) + \tau_{\rm cc}(p)] + \pi + \phi_n \; .\end{aligned} \tag{9}$$

When deriving Eq. (9), we made the following simplifications. In our simulations, $\Delta\phi_{2q\pm1} = \pi$ and the harmonic phase difference in RABBITT and uRABBITT cancels. Another simplification made in Eq. (9) exploits the fact that the Wigner and CC phases add up to a constant near the threshold. This is clearly seen in the top row of panels in Fig. 3 where the RABBITT phase remains flat before making cross-over to the uRABBITT regime. Therefore, $\tau_{\rm W}(k) + \tau_{\rm cc}(k) \approx \tau_{\rm W}(p) + \tau_{\rm cc}(p)$ and the corresponding terms in the RABBITT and uRABBITT phases cancel. Finally, the orbital momentum factor $\phi_{L\lambda}$ is evaluated under assumption of the Fano propensity rule for the dipole transition $L - \lambda = 1$ [24, 36]. It is this propensity rule that enhances strongly the f partial wave in the final continuum. This explains a sharp drop of the uRABBITT phase near a kinematic node of Y_{30} in Eq. (3). Predictions of Eq. (9) are marked in Fig. 2b and are found in good agreement with non-perturbative TDSE calculations. The experimental data of [28] are overplotted in Fig. 2a. We clearly see that this measurement covers only a small part of the RABBITT phase transition and corresponds to the resonant term ϕ_n in Eq. (9).

In summary, we studied systematically the RABBITT phase variation near the ionization threshold in He and Ne at 800 nm. When one of the harmonics (H15 in He and H13 in Ne) crosses the ionization threshold, the next upward sideband (SB16 in He and SB14 in Ne) is formed by interference of the continuous transition with a discrete one from the resonant bound state ($1s3p$ in He and $2p^5 3d$ in Ne). This corresponds to the cross-over to the uRABBITT regime and a π jump of the RABBIT phase. An additional smooth variation of the uRABBIT phase is related to the resonant phase of the two-photon matrix element dependent on the detuning relative to corresponding bound state. This resonant phase has been modeled theoretically [37, 38] and measured in [28]. Above the threshold, the RABBITT phase remains a smooth function of the photoelectron energy and can be extrapolated to the limit $E \to 0$ where the atomic time delay remains small $\tau_a(E \to 0) \simeq -40$ as in He and -35 as in Ne (the slope of the solid line in Fig. 2a and Fig. 2b, respectively). At the same time, both constituents of the atomic time delay $\tau_{\rm W}$ and $\tau_{\rm cc}$ are divergent near threshold and a simple extrapolation of $\tau_{\rm cc}(E \to 0)$ from hydrogenic values [25] at finite E is not valid. Because $\tau_{\rm W}(E \to 0)$ is known analytically from Eq. (8) and $\tau_a(E \to 0)$ is small, the second constituent of the atomic time delay $\tau_{\rm cc}(E \to 0)$ can be established accurately. In particular, $\tau_{\rm cc} = -56 \pm 0.2$ fs for SB14 in Ne ($E = 0.14$ eV) [41]. The compensation of the Wigner and CC phases and corresponding time delays near the threshold has already been noted in a THz AS experiment [39]. The spectral width of our APT allowed us to study the passage of the uRABBITT harmonic over a well isolated bound state ($1s3p$ in He and $2^5 3d$ in Ne). An improved APT spectral resolution would facilitate probing more narrowly spaced energy levels thus making uRABBITT a sensitive probe of the bound state structure of the target atom. This development is currently underway [29].

We gratefully acknowledge Giuseppe Sansone, Hamed Ahmadi and Matteo Moioli for drawing our attention to the uRABBITT phenomenon and discussing with us their experimental findings. We thank Thomas Pfeiffer and Robert Moshammer for critical reading of, and commenting on, the manuscript. Serguei Patchkovskii is acknowledged for placing his iSURF TDSE code at our disposal. Resources of National Computational Infrastructure facility (NCI Australia) have been employed.

[1] U. Fano, *Effects of configuration interaction on intensities and phase shifts*, Phys. Rev. **124**, 1866 (1961).

[2] D. Finkelstein-Shapiro and A. Keller, *Ubiquity of Beutler-Fano profiles: From scattering to dissipative processes*, Phys. Rev. A **97**, 023411 (2018).

[3] A. N. Poddubny, M. V. Rybin, M. F. Limonov, and Y. S. Kivshar, *Fano interference governs wave transport in disordered systems*, Nature Communications **3**, 914 (2012).

[4] M. F. Limonov, M. V. Rybin, A. N. Poddubny, and Y. S. Kivshar, *Fano resonances in photonics*, Nature Photonics **11**, 543 (2017).

[5] U. Fano and J. W. Cooper, *Spectral distribution of atomic oscillator strengths*, Rev. Mod. Phys. **40**, 441 (1968).

[6] M. Wellner, *Levinson's theorem (an elementary derivation)*, American Journal of Physics **32**(10), 787 (1964).

[7] L. Rosenberg, *Levinson-Seaton theorem for potentials with an attractive Coulomb tail*, Phys. Rev. A **52**(5), 3824 (1995).

[8] M. Schultze, M. Fiess, N. Karpowicz, J. Gagnon, M. Korbman, M. Hofstetter, S. Neppl, A. L. Cavalieri, Y. Komninos, T. Mercouris, et al., *Delay in photoemission*, Science **328**, 1658 (2010).

[9] P. M. Paul, E. S. Toma, P. Breger, G. Mullot, F. Aug, P. Balcou, H. G. Muller, and P. Agostini, *Observation of a train of attosecond pulses from high harmonic generation*, Science **292**(5522), 1689 (2001).

[10] Y. Mairesse, A. de Bohan, L. J. Frasinski, H. Merdji, L. C. Dinu, P. Monchicourt, P. Breger, M. Kovacev, R. Taïeb, B. Carré, et al., *Attosecond synchronization of high-harmonic soft x-rays*, Science **302**(5650), 1540 (2003).

[11] K. Klünder, J. M. Dahlström, M. Gisselbrecht, T. Fordell, M. Swoboda, D. Guénot, P. Johnsson, J. Caillat, J. Mauritsson, A. Maquet, et al., *Probing single-photon ionization on the attosecond time scale*, Phys. Rev. Lett. **106**, 143002 (2011).

[12] R. Pazourek, S. Nagele, and J. Burgdörfer, *Time-resolved photoemission on the attosecond scale: opportunities and challenges*, Faraday Discuss. **163**, 353 (2013).

[13] M. Huppert, I. Jordan, D. Baykusheva, A. von Conta, and H. J. Wörner, *Attosecond delays in molecular photoionization*, Phys. Rev. Lett. **117**, 093001 (2016).

[14] J. Vos, L. Cattaneo, S. Patchkovskii, T. Zimmermann, C. Cirelli, M. Lucchini, A. Kheifets, A. S. Landsman, and U. Keller, *Orientation-dependent stereo Wigner time delay in a small molecule*, Science **360**(6395), 1326 (2018).

[15] M. Ossiander, J. Riemensberger, S. Neppl, M. Mittermair, M. Schäffer, A. Duensing, M. S. Wagner, R. Heider, M. Wurzer, M. Gerl, et al., *Absolute timing of the photoelectric effect*, Nature **561**, 374 (2018).

[16] D. Guénot, K. Klünder, C. L. Arnold, D. Kroon, J. M. Dahlström, M. Miranda, T. Fordell, M. Gisselbrecht, P. Johnsson, J. Mauritsson, et al., *Photoemission-time-delay measurements and calculations close to the 3s-ionization-cross-section minimum in ar*, Phys. Rev. A **85**, 053424 (2012).

[17] M. Isinger, R. Squibb, D. Busto, S. Zhong, A. Harth, D. Kroon, S. Nandi, C. L. Arnold, M. Miranda, J. M. Dahlström, et al., *Photoionization in the time and frequency domain*, Science **358**, 893 (2017).

[18] I. Jordan, M. Huppert, S. Pabst, A. S. Kheifets, D. Baykusheva, and H. J. Wörner, *Spin-orbit delays in photoemission*, Phys. Rev. A **95**, 013404 (2017).

[19] D. Guénot, D. Kroon, E. Balogh, E. W. Larsen, M. Kotur, M. Miranda, T. Fordell, P. Johnsson, J. Mauritsson, M. Gisselbrecht, et al., *Measurements of relative photoemission time delays in noble gas atoms*, J. Phys. B **47**(24), 245602 (2014).

[20] C. Palatchi, J. M. Dahlstrm, A. S. Kheifets, I. A. Ivanov, D. M. Canaday, P. Agostini, and L. F. DiMauro, *Atomic delay in helium, neon, argon and krypton*, J. Phys. B **47**(24), 245003 (2014).

[21] A. Jain, T. Gaumnitz, A. Kheifets, and H. J. Wörner, *Using a passively stable attosecond beamline for relative photoemission time delays at high XUV photon energies*, Opt. Express **26**(22), 28604 (2018).

[22] S. Heuser, A. Jiménez Galán, C. Cirelli, C. Marante, M. Sabbar, R. Boge, M. Lucchini, L. Gallmann, I. Ivanov, A. S. Kheifets, et al., *Angular dependence of photoemission time delay in helium*, Phys. Rev. A **94**, 063409 (2016).

[23] C. Cirelli, C. Marante, S. Heuser, C. L. M. Petersson, A. J. Galán, L. Argenti, S. Zhong, D. Busto, M. Isinger, S. Nandi, et al., *Anisotropic photoemission time delays close to a Fano resonance*, Nature Comm. **9**, 955 (2018).

[24] D. Busto, J. Vinbladh, S. Zhong, M. Isinger, S. Nandi, S. Maclot, P. Johnsson, M. Gisselbrecht, A. L'Huillier, E. Lindroth, et al., *Fano's propensity rule in angle-resolved attosecond pump-probe photoionization*, Phys. Rev. Lett. **123**, 133201 (2019).

[25] J. Dahlström, D. Guénot, K. Klünder, M. Gisselbrecht, J. Mauritsson, A. L. Huillier, A. Maquet, and R. Taïeb, *Theory of attosecond delays in laser-assisted photoionization*, Chem. Phys. **414**, 53 (2012).

[26] A. Harth, N. Douguet, K. Bartschat, R. Moshammer, and T. Pfeifer, *Extracting phase information on continuum-continuum couplings*, Phys. Rev. A **99**, 023410 (2019).

[27] J. Fuchs, N. Douguet, S. Donsa, F. Martin, J. Burgdörfer, L. Argenti, L. Cattaneo, and U. Keller, *Time delays from one-photon transitions in the continuum*, Optica **7**, 154 (2020).

[28] M. Swoboda, T. Fordell, K. Klünder, J. M. Dahlström, M. Miranda, C. Buth, K. J. Schafer, J. Mauritsson, A. L'Huillier, and M. Gisselbrecht, *Phase measurement of resonant two-photon ionization in helium*, Phys. Rev. Lett. **104**, 103003 (2010).

[29] G. Sansone, H. Ahmadi, and M. Moioli (2020), private communication.

[30] M. Y. Amusia, *Atomic photoeffect* (Plenum Press, New York, 1990).

[31] F. Morales, T. Bredtmann, and S. Patchkovskii, *iSURF: a family of infinite-time surface flux methods*, J. Phys. B **49**(24), 245001 (2016).

[32] I. A. Ivanov and A. S. Kheifets, *Angle-dependent time delay in two-color XUV+IR photoemission of He and Ne*, Phys. Rev. A **96**, 013408 (2017).

[33] A. W. Bray, F. Naseem, and A. S. Kheifets, *Simulation of angular-resolved RABBITT measurements in noble-gas atoms*, Phys. Rev. A **97**, 063404 (2018).

[34] V. Véniard, R. Taïeb, and A. Maquet, *Phase dependence of $(n+1)$-color $(n>1)$ ir-uv photoionization of atoms with higher harmonics*, Phys. Rev. A **54**, 721 (1996).

[35] J. C. A. Barata, L. F. Canto, and M. S. Hussein, *New asymptotic formulae for the point Coulomb phase shift*, Brazilian J. Phys. **41**, 50 (2011).

[36] U. Fano, *Propensity rules: An analytical approach*, Phys. Rev. A **32**, 617 (1985).

[37] A. Jiménez-Galán, F. Martín, and L. Argenti, *Two-photon finite-pulse model for resonant transitions in attosecond experiments*, Phys. Rev. A **93**, 023429 (2016).

[38] K. L. Ishikawa and K. Ueda, *Competition of reso-*

nant and nonresonant paths in resonance-enhanced two-photon single ionization of He by an ultrashort extreme-ultraviolet pulse, Phys. Rev. Lett. **108**, 033003 (2012).

[39] G. Schmid, K. Schnorr, S. Augustin, S. Meister, H. Lindenblatt, F. Trost, Y. Liu, N. Stojanovic, A. Al-Shemmary, T. Golz, et al., *Terahertz-field-induced time shifts in atomic photoemission*, Phys. Rev. Lett. **122**, 073001 (2019).

[40] See Secton A of Supplementary Material for derivation

[41] See Section B of Supplementary Material for detail

RABBITT phase transition across the ionization threshold
Supplementary material

Anatoli S. Kheifets and Alexander W. Bray

Research School of Physics and Engineering,

The Australian National University, Canberra ACT 0200, Australia

A. Resonant phase for a finite spectral width

We conduct the time integration in the matrix element of two-photon ionization with monochromatic XUV Ω and IR ω fields

$$D^{(2)}(\Omega,\omega) \propto \int_{-\infty}^{\infty} dt_1 e^{it_1(\Omega+E_i-E_n)} \int_{t_1}^{\infty} dt_2 e^{it_2(\omega+E_n-E)}$$

We change variables $t_1 = t_2 + t_1 - t_2 \equiv t_2 + \tau$ where $\tau \le 0$ and transform the integral:

$$\begin{aligned} D^{(2)}(\Omega,\omega) \;&\propto \int_{-\infty}^{\infty} dt_2 e^{it_2(\Omega+E_i-\cancel{E_n}+\omega+\cancel{E_n}-E)} \int_{-\infty}^{0} d\tau e^{i\tau(\Omega+E_i-E_n)} \\ &\propto \frac{1}{\Omega+E_i-E_n-i\delta} \quad \times \delta(\Omega+\omega+E_i-E) \end{aligned}$$

We added an infinitesimal $\delta > 0$ to the energy denominator to make sure the integral converges at $\tau \to -\infty$.

With a decaying XUV field $\exp(i\Omega t)\exp(-\Gamma t)$ the energy denominator becomes

$$\frac{1}{\Omega+E_i-E_n-i\Gamma} \equiv \frac{1}{\Delta-i\Gamma} = \frac{\Delta+i\Gamma}{\Delta^2+\Gamma^2} \quad , \text{ where } \; \Delta \equiv \Omega+E_i-E_n \text{ is detuning}$$

The resonant phase shift

$$\phi_r = \arg\left[D^{(2)}(\Omega,\omega)\right] = \arctan\frac{\Gamma}{\Delta}$$

With a Gaussian envelope $\exp(i\Omega t)\exp(-at^2)$, the τ integration leads to

$$\int_{-\infty}^{0} d\tau e^{-i\Delta\tau} e^{-a\tau^2} = \int_{0}^{\infty} d\tau e^{-a\tau^2}\cos\Delta\tau - i\int_{0}^{\infty} d\tau e^{-a\tau^2}\sin\Delta\tau \equiv C - iS \quad , \quad \phi_r = \arctan\frac{S}{C}$$

According to Gradshteyn and Ryzhik [1] Eq. 3.896, p. 480

$$C = \int_0^{\infty} e^{-ax^2}\cos\,bx\,dx = \frac{1}{2}\sqrt{\frac{\pi}{a}}\exp\left(-\frac{b^2}{4a}\right) \quad , \quad S = \int_0^{\infty} e^{-ax^2}\sin\,bx\,dx = \frac{b}{2a}\sum_{k=1}^{\infty}\frac{1}{(2k-1)!!}\left(-\frac{b^2}{2a}\right)^{k-1}$$

For a small de-tuning $\Delta/a \equiv b/a \ll 1$ and

$$C = \frac{1}{2}\sqrt{\frac{\pi}{a}} \quad , \quad S = \frac{b}{2a} \quad , \quad \phi_r = \frac{S}{C} = \arctan\left[\frac{b}{2a} 2\sqrt{\frac{a}{\pi}}\right] = \arctan\frac{b}{\sqrt{\pi a}} = \arctan\frac{1}{\sqrt{\pi}}\frac{\Delta}{\Gamma}$$

Here the spectral width $\Gamma = \sqrt{a}$.

More eleborate expressions for the resonant two-photon absorption phase are derived in [2, 3]

B. Wigner time delay uncertainty at the threshold

The bare Coulmp phase approximation may be too crude. So we evaluate the elastic scattering phases numerically using the ATOM computer code [4]. These phases produce the time delays that vary slightly in different photoemission channels as shown in Fig. S1 . This difference provides an error estimate of the Wigner time delay.

FIG. S1 : Wigner time delay in various photoionization channels of Ne extrapolated to the momentum $\kappa_0 = 0.1$ eV (the photoelectron energy $E_0 = 0.14$ eV) corresponding to the $3d$ resonance in Ne.

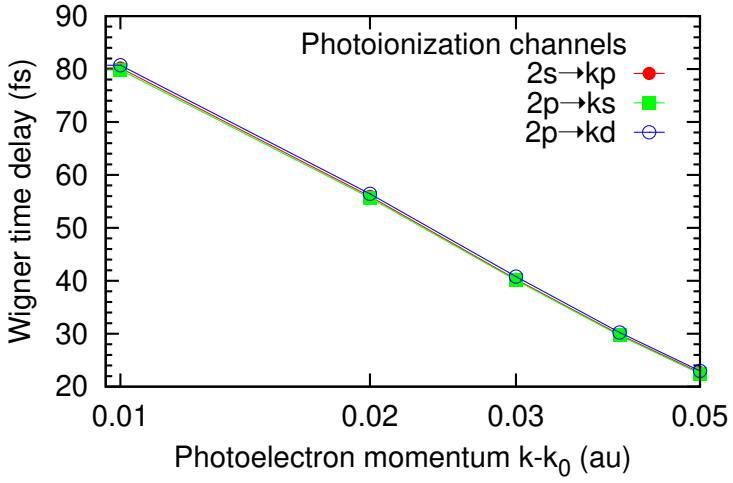

[1] I. Gradshteyn and I. Ryzhik, *Table of Integrals, Series, and Products* (Elsevier Science, 2014).

[2] A. Jiménez-Galán, F. Martín, and L. Argenti, *Two-photon finite-pulse model for resonant transitions in attosecond experiments*, Phys. Rev. A **93**, 023429 (2016).

[3] K. L. Ishikawa and K. Ueda, *Competition of resonant and nonresonant paths in resonance-enhanced two-photon single ionization of He by an ultrashort extreme-ultraviolet pulse*, Phys. Rev. Lett. **108**, 033003 (2012).

[4] M. I. Amusia and L. V. Chernysheva, *Computation of atomic processes : A handbook for the ATOM programs* (Institute of Physics Pub., Bristol, UK, 1997).